JOURNAL OF Applied Polymer SCIENCE

Film-Forming Behavior and Mechanical Properties of Colloidal Silica/Polymer Latex Blends with High Silica Load

Ling Yang, Shuxue Zhou, Guangxin Gu, Limin Wu
Department of Materials Science, Advanced Coatings Research Center of Ministry of Education of China, Fudan University, Shanghai 200433, People's Republic of China
Correspondence to: S. Zhou (E-mail: zhoushuxue@fudan.edu.cn)

ABSTRACT: In this article, silica sol (diameter: 8–100 nm) and polymer latex ($T_g < 25°C$) were mixed and dried at room temperature to prepare nanocomposite films with high silica load (≥50 wt %). Effects of silica size, silica load, and the T_g of the polymer on the film-forming behavior of the silica/polymer latex blend were investigated. The transparency, morphology, and mechanical properties of the nanocomposite films were examined by UV–Vis spectroscopy, SEM, and nanoindentation tests, respectively. Transparent and crack-free films were produced with silica loads as high as 70 wt %. Thirty nanometers was found to be the critical silica size for the evolution of film-forming behavior, surface morphology, and mechanical properties. Colloidal silica particles smaller than this critical size act as binders to form strong silica skeleton. This gives the final silica/polymer nanocomposite film its porous surface and high mechanical strength. However, silica particles with sizes of 30 nm or larger tend to work as nanofillers rather than binders, causing poor mechanical strength. We also determined the critical silica load appeared for the mechanical strength of silica/polymer film at high silica load. © 2012 Wiley Periodicals, Inc. J. Appl. Polym. Sci. 129: 1434–1445, 2013

KEYWORDS: colloids; blends; mechanical properties; morphology; films

Received 31 April 2012; accepted 12 November 2012; published online 12 December 2012
DOI: 10.1002/app.38827

INTRODUCTION

Blending hard and soft colloidal particles is one of the simplest ways to produce nanocomposite films, which show well film formation characteristics, desired hardness, elastic modulus, and enhanced block resistance.[1,2] It is especially promising as an alternative strategy for the fabrication of low-volatile organic compounds (VOC) latex coatings by decreasing or even avoiding the use of coalescing agents.[3] Because of these advantages, films from blends of soft and hard colloidal particles have received a variety of academic and industrial attention over the past several years. These hard particles could be polymer particles with high T_g[2–7]and ceramic nanoparticles.[8] Particularly, the ceramic nanoparticles can additionally endow the films with enhanced solvent resistance, weathering resistance, and thermal stability, because of their excellent resistances to chemicals, heat, and UV irradiation. The ceramic nanoparticles mostly involved are colloidal silica particles.

A few reports have been paid on blending of polymer latex with colloidal silica particles over the past decade.[9,10] Winnik and coworker studied the polymer interdiffusion in poly(butyl methacrylate)/silica composite films with colloidal silica.[11] Wada et al. prepared waterborne organic–inorganic composite films with high stain resistance from blends of silane hybridized acrylic latex with colloidal silica.[12,13] Liao et al. prepared nanocomposite latex by directly mixing the triethoxysilyl group-bearing polyacrylate latex with colloidal silica.[14] We have prepared nanocomposite latex by blending P (styrene-*co*-butyl acrylate-*co*-acrylic acid) latex with an acidic silica sol with silica content up to 34 wt % in the dried film.[15] Among these reports, colloidal silica particles merely acted as nanofiller to increase the hydrophilicity, mechanical strength, or solvent resistance of the final polymer latex films. Recently, we fabricated three-dimensional ordered porous polymer films from blends of monodisperse polyacrylate latex and silica sol through what we have called forced-drying strategy.[16–18] Colloidal silica particles therein worked as the inorganic skeleton of the porous films. To be disappointed, all these blends of polymer latex and silica sol involved generally have silica loads less than 40 wt % in their dried films.

However, silica-enriched films are highly desirable because they have potential applications in hard coatings, flame-retardant coatings, low CTE (coefficient of thermal expansion) coatings and heat-resistant coatings.[19–26] However, silica-dominated nanocomposite coatings are nearly all fabricated from sol-gel

Table I. Characteristics of Silica Sols

Name of silica sol	Commercial name	Particle size[a] (nm)	Solid content (%)	pH	Manufacturer
S8	AJN-830	8 (9)	30	9.0–10.5	Foshan Zhongfa Sodium Silicate Company, China
S14	AJN-1430	14 (15)	30	9.0–10.5	Foshan Zhongfa Sodium Silicate Company, China
S20	NYACOL 20/40	20 (24)	40	9.7–10.0	Shanghai Seebio Biotechnology, China
S30	D20:30%	30 (35)	30	9.0–10.0	Shandong Peak-tech New Materials, China
S50	LS50:30%	50 (59)	30	9.0–10.0	Shandong Peak-tech New Materials, China
S80	LS80:30%	80 (98)	30	9.0–10.0	Shandong Peak-tech New Materials, China
S100	LS100:30%	100 (117)	30	9.0–10.0	Shandong Peak-tech New Materials, China

[a]The data in the bracket are the *Z*-average particle size as determined in our lab.

processes involving tetraethoxysilane (TEOS) or tetramethoxysilane (TMOS), which are rather expensive and create VOC due to release of alcohol. In contrast, the colloidal-silica-particle-based route for fabrication of silica-enriched coatings with high silica load (>50%) has only seldom been reported. Martinez and Lewis[27] ever monitored the shape evolution and stress development in the silica range of 20–100% while Singh et al.[28] concerned the cracking behavior of colloidal silica/polyacrylate latex blend within the entire range of volume fraction (0–1). Whatever, big silica particle of 570 and 330 nm were correspondingly adopted in their studies. We deduce that these films are lack of mechanical strength at high silica load since the silica microspheres therein only act as filler in the composite films.

To develop a cheap route for acquiring silica-rich nanocomposite coatings with good mechanical strength, the film-forming and mechanical behaviors of silica/polymer latex blends with small silica particles (size range: 8–100 nm) and high silica load (≥50 wt %) were systematically investigated in this article. A critical silica size was found for the evolution of film-forming behavior, surface morphology, and mechanical properties. Transparent and crack-free films were successfully achieved with silica loads as high as 70 wt %.

EXPERIMENTAL

Materials

All silica sols and polymer latexes are commercial products. Tables I and II summarize their commercial names, main properties and Manufacturers. For the convenience of description in the text, both silica sols and polymer latex are renamed as SX and PY where X and Y represent the particle size of silica sol and the T_g of polymer latexes, respectively. Except for P6 latex, which is nanosize, all latexes have nearly the same particle size. The silica sols were further observed by transmission electronic microscope, as shown in Figure 1. Except for S100, the colloidal silica sols used have narrow particle size distribution.

Preparation of Silica/Polymer Nanocomposite Films

Silica/polymer latex blends were prepared by mixing silica sol with polymer latex and sonicating at room temperature for about 15 min. All blends were adjusted to 30 wt % to cast films by No.4 standard coating bar (wetting film thickness: 40 μm) using a R K Control Coater (R K Print Coat Instruments Ltd, UK) and dried for 24 h in an oven of 25°C and relative humidity of 50%. Mass fraction of silica in dried film (f) was calculated using the following equation:

$$f = \frac{m_{\text{silica}} \times C_{\text{silica}}}{m_{\text{resin}} \times C_{\text{resin}} + m_{\text{silica}} \times C_{\text{silica}}} \quad (1)$$

Here m_{silica} and m_{resin} are the masses of silica sol and polymer latex in the blends, and C_{silica} and C_{resin} are the solid contents of silica sol and polymer latex. Three series of silica/polymer blends were mainly fabricated: latex P6 with various silica sols (S8–S100), silica sol S14 with various polymer latexes (P-22–P25), and silica sol S50 with various polymer latexes (P-22–P25).

Characterization

The silica particles were observed with a transmission electron microscope (TEM, HitachiH-800, Hitachi Corp.). The silica sols were diluted with deionized water and then dried onto carbon-coated copper grids before examination. The particle sizes of colloidal silica sol and polymer latex were determined by Nano ZS90 particle size analyzer (Malvern, UK). *Z*-average size was adopted. The cracking behavior of the films was assessed using both naked eyes and a KH-7700 digital microscope (HIROX, Japan).

The transmission spectra of films in the wavelength range of 200–800 nm were recorded on a UV–Vis spectrophotometer (UV-4100, Hitachi). The scanning speed was set as 300 nm min^{-1}.

The morphologies of crack-free films were observed with a scanning electron microscope (Superscan SSX-550, Shimadzu,

Table II. Properties of Polymer Latexes

Name	Commercial name	Composition	Solid content (%)	T_g (°C)	MFFT[a] (°C)	pH	Particle size[b] (nm)	PDI[b]	Manufacturer
P6	R-64	Styrene-acrylic	30	6	<5	8.5	51	0.128	Dow chemical
P-22	BLJ-968M	Acrylic latex	50	−22	0	7.0-9.0	153	0.04	Shanghai Bao-Li-Jia Chemical, China
P-3	SF055	Styrene-acrylic	47.5	−3	0	7.0-9.0	133	0.004	Dow chemical
P1	1050LOE	Acrylic latex	50	1	2	9.0	114	0.122	Dow chemical
P12	VSR-50	Acrylic latex	45.5	12	-	8.0-9.0	121	0.06	Dow chemical
P25	AC-268	Acrylic latex	45.5	25	14	7.0-9.0	120	0.078	Dow chemical

[a]Minimum film formation temperature.
[b]Z-average particle size and particle size distribution as determined in our lab.

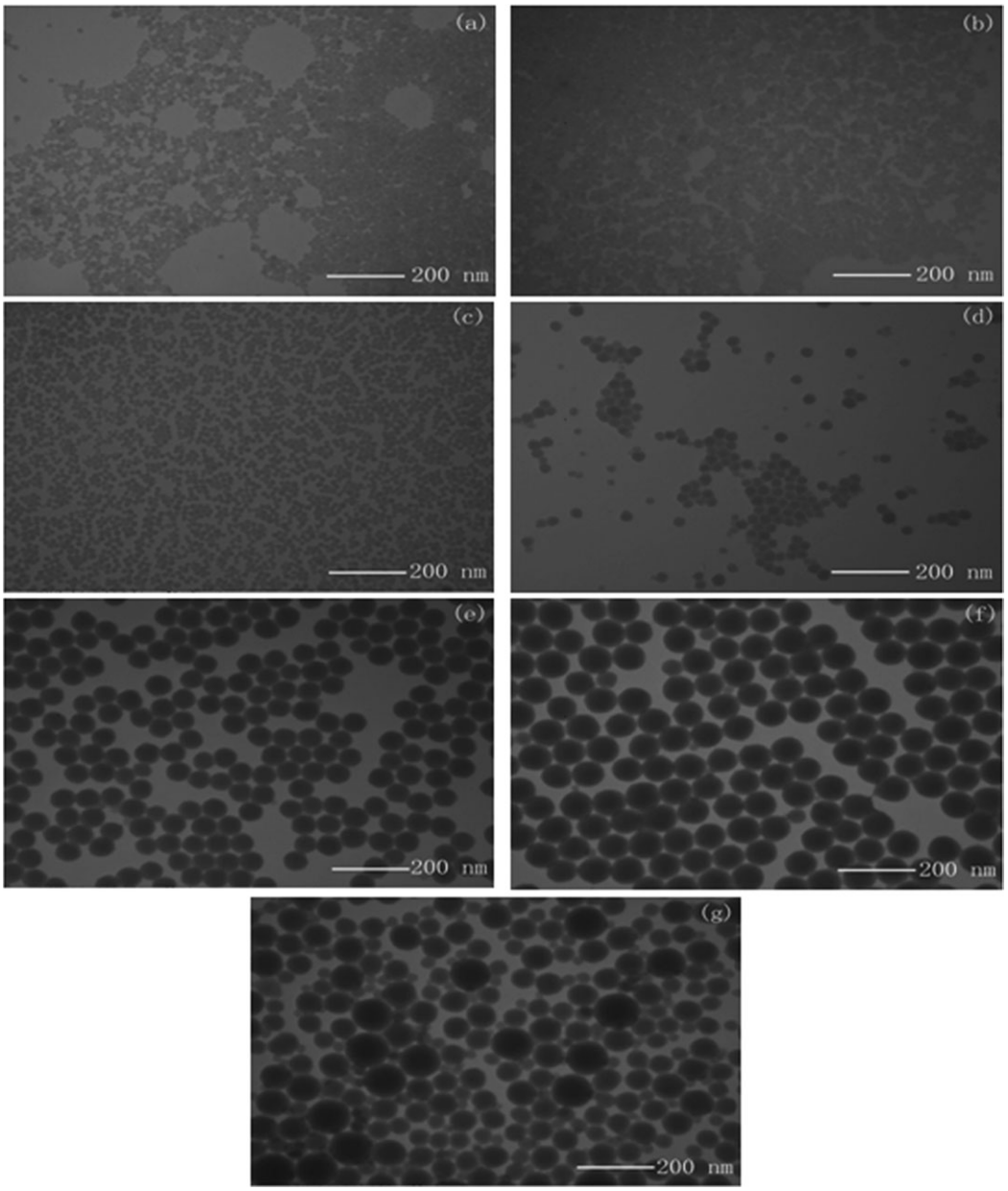

Figure 1. The TEM images of the silica sols used: (a) S8, (b) S14, (c) S20, (d) S30, (e) S50, (f) S80, and (g) S100.

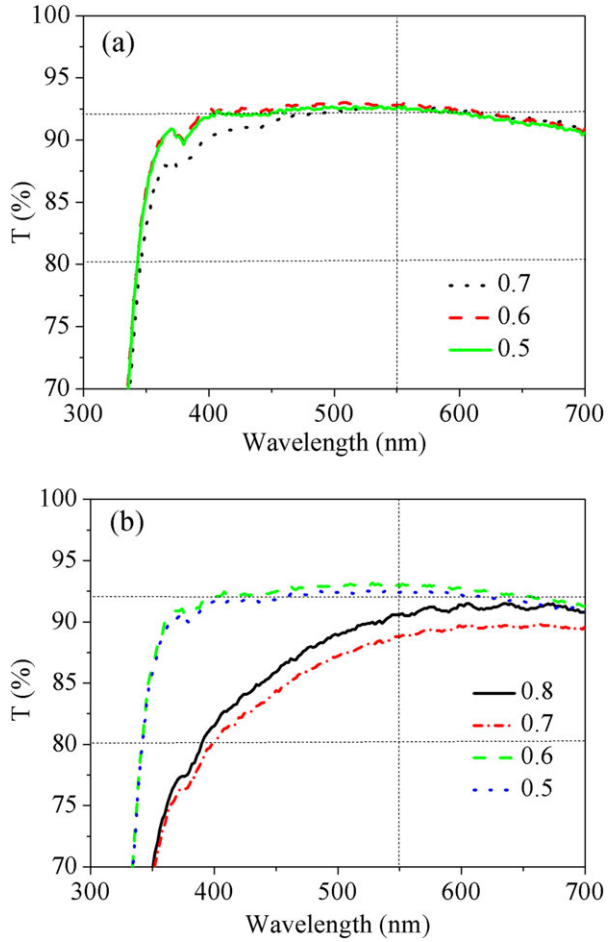

Figure 2. UV–vis transmittance spectra of crack-free films with different f formed from (a) S14/P6 blend and (b) S30/P6 blend. (Dashed lines are guidelines only). [Color figure can be viewed in the online issue, which is available at wileyonlinelibrary.com.]

Japan) at an accelerating voltage of 10 kV. The cross-section of the sample for SEM observation was obtained through brittle fracture in liquid nitrogen. All samples were sputtering-coated with Au prior to observation.

The nanoindentation tests were carried out using an ultra nano-indentation tester (CSM Instruments, Switzerland) with a Berkovich diamond indenter. After making contact with the surface, the indenter was penetrated into the coating at a constant strain rate of 0.05 s^{-1} until it reached a depth of 500 nm. The intender was maintained at the maximum load for 50 s and then withdrawn from the surface at the same rate as loading. At least 5 indents were performed per sample and average values were adopted. The hardness (H) and elastic modulus (E) were calculated from the unloading curve using the Oliver and Pharr method.[29] The equations are as follows:

$$H = \frac{P_{\max}}{A} \tag{2}$$

$$S = 2\beta\sqrt{\frac{A}{\pi}}E_r \tag{3}$$

where $P_{\max}$ is the maximum load and A the projected contact area; S is the contact stiffness of the material, which is defined as the initial load–displacement slope of the unloading curve; β is a constant depending on the geometry of the indenter, and E_r the reduced elastic modulus based on the following relationship:

$$\frac{1}{E_r} = \frac{1-\nu^2}{E} + \frac{1-\nu_i^2}{E_i} \tag{4}$$

where E_i (1140 GPa) and ν_i (0.07) are the elastic modulus and Poisson's ratio of the diamond indenter, respectively, and E and ν are the elastic modulus and Poisson's ratio of the sample, respectively.

RESULTS AND DISCUSSION

Film Formation of Colloidal Silica/Polymer Latex Blends

The ability of silica/polymer latex blends to form films was ascertained based on cracks (macro- and micro-cracks) and film transparency. If transparent and crack-free films were obtained, the corresponding latex blends were considered to have good film-forming ability. Otherwise, the corresponding latex blends were regarded as having poor film-forming performance. Similar criterion was adopted in Lepizzera et al.'s report on the film-forming ability of hard/soft polymer latex blends.[2] Cracks can be easily examined with both naked eyes and an optical microscope. Nevertheless, the absolute transmission of the film that can be regarded as transparent film is not usually given. Feng et al. ever defined that the polymer blend latex films with transmissions of 85–95% and 5–20% correspond to transparent films and turbid films.[3] But, in our case, the optical transmission difference of the composite films at various silica/polymer ratios was not significant, although their film-forming behavior obviously varied. To distinguish the small change of the transparency, the optical transparency of the nanocomposite film was quantitatively determined using a UV–Vis spectrophotometer. Figure 2 shows typical UV–Vis spectra of S14/P6 and S30/P6 blend films with different silica loads. The crack-free S14/P6 films with f among 0.5 to 0.7 are transparent, with transmission of 92.5% at a wavelength of 550 nm. The crack-free S30/P6 films showed the same high level of transparency, at $f = 0.5$ and 0.6, but showed less transparency at $f = 0.7$ (transmission: 88.8%) and 0.8 (transmission: 90.5%). Crack-free translucent film was therefore defined as the film with a transmission of 80–90% at 550 nm and crack-free transparent film was defined as film with transmission above 92% at 550 nm. Herein, the maximum mass fraction of silica was defined as f_1 and f_2 for the formation of crack-free film and crack-free/transparent film, respectively, under given drying conditions (25°C, 50% RH). Both of these were adopted to describe the film-forming behavior of silica/polymer latex blends in our study.

Effects of Fraction and Size of Silica Sol. All silica sols used here were unable to form crack-free film when used alone, even if the wet film thickness was reduced to 6 μm (about 1–1.5 μm in dry film thickness). However, if a certain amount of polymer latex was added, the film-formation of silica sol was greatly improved. Nevertheless, the film-forming behavior was found to be strongly-dependent on f and on the size of silica sol. Figure 3 displays the film-forming ability of silica/polymer latex blends

Applied Polymer SCIENCE

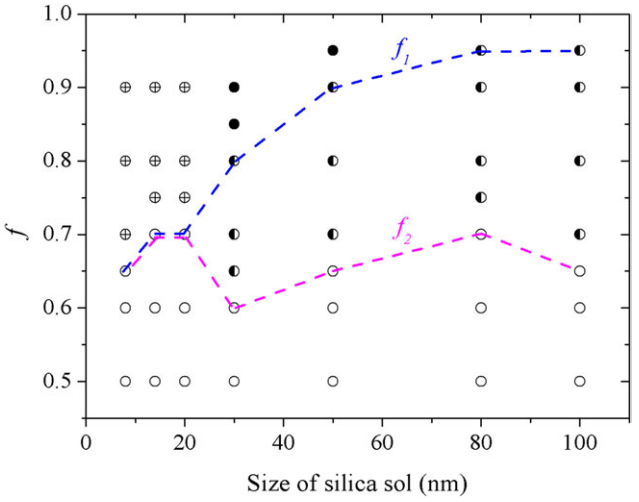

Figure 3. Film-forming ability of silica/polymer latex blend prepared from P6 latex and silica sol with various sizes and fractions. (○: crack-free transparent film ◐: crack-free translucent film, ⊕: cracked transparent film, ●: cracked translucent film; f_1: blue dash line, f_2: magenta dash line). [Color figure can be viewed in the online issue, which is available at wileyonlinelibrary.com.]

prepared from P6 latex and various silica sols. For those blends with 8, 14, and 20 nm silica sols, crack-free transparent films directly transformed into crack film when f was beyond the critical fraction of silica. As f increased, additional transition from crack-free transparent film to crack-free translucent film was observed for blends with 30, 50, 80, and 100 nm silica sols before cracking took place. High fractions of soft polymer latex were found to favor film formation of silica/polymer latex blend, being analogs to the film-forming behavior of hard polymer/soft polymer latex blends.

Figure 2 also shows that f_1 increases gradually but f_2 changes little as the size of silica sol increases. f_2 of 0.6–0.7 (volume fraction of 0.44–0.55 at densities of 2.2 and 1.17 g/cm^3, which was correspondingly adopted for colloidal silica and polymer particles) remained nearly the same as the critical volume fractions of hard polymer particle reported for formation of transparent hard/soft polymer latex blend films.[2–5] However, the findings of these various reports and the current study with respect to the sizes of hard and soft particles and the film thickness were completely different.[2–5] In our study, f_1 was found to reach values up to 0.95 (volume fraction: 0.91) for 80 and 100 nm silica sols.

The cracking of silica/polymer nanocomposite film should be caused by the failed releasing of internal stress in the film.[5,27] It is well known that the internal stress can be generated by water evaporation and capillary force.[30,31] In our case, silica particles are rather small. They have high surface free energy and a lot of silanol groups at their surface, and thus can interact with each other via van der Waals, hydrogen bond, and even chemical bond via the condensation of surface silanol groups. The silica particle interaction herein will be stemmed as other source of internal stress in the silica/polymer nanocomposite film. The strong silica interaction also leads to the formation of silica particle network. Nevertheless, the easy cracking of pure silica particle film suggests that the strength of silica particle network can not resist the internal stress generated during film formation of colloidal silica. Therefore, the internal stress has to be released mainly by the soft latex particle deformation. As f increases, the stress resistance decreases due to lower fractions of soft polymer, finally causing cracks.

The evolution of f_1 with silica size may be mainly explained by the capillary tension that developed from the capillary pressure (P_{cap}) in the pore liquid.[32] The capillary pressure can be estimated from the equation, $P_{cap} = -2\gamma/R_M$, where R_M is the radius of curvature of the nanomenisci and γ is the surface tension of the air-water interface. When colloidal silica particles are closely packed, R_M can be as small as the minimum pore radius, namely, $0.15R$ (R-the particle radius).[33] That is, as silica size increases, P_{cap} decreases. It means that the minimum quantity of soft polymer binder needed to resist cracking reduces. In other words, f_1 increases with increasing silica size.

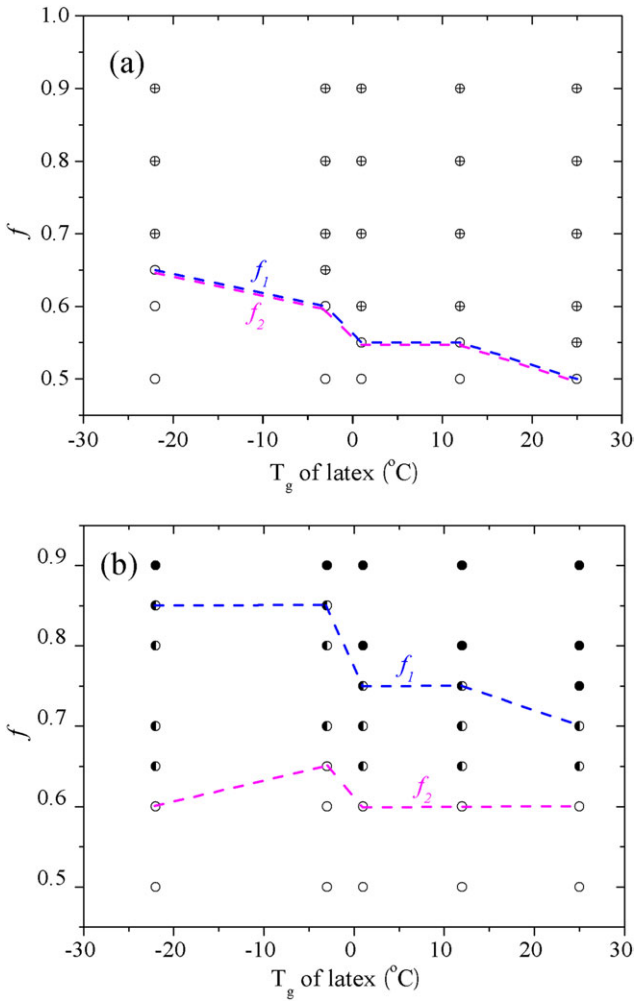

Figure 4. The film-forming ability of (a) S14/polymer latex blend and (b) S50/polymer latex blends. (○: crack-free transparent film, ◐: crack-free translucent film, ⊕: cracked transparent film, ●: cracked translucent film; f_1: blue dash line, f_2: magenta dash line). [Color figure can be viewed in the online issue, which is available at wileyonlinelibrary.com.]

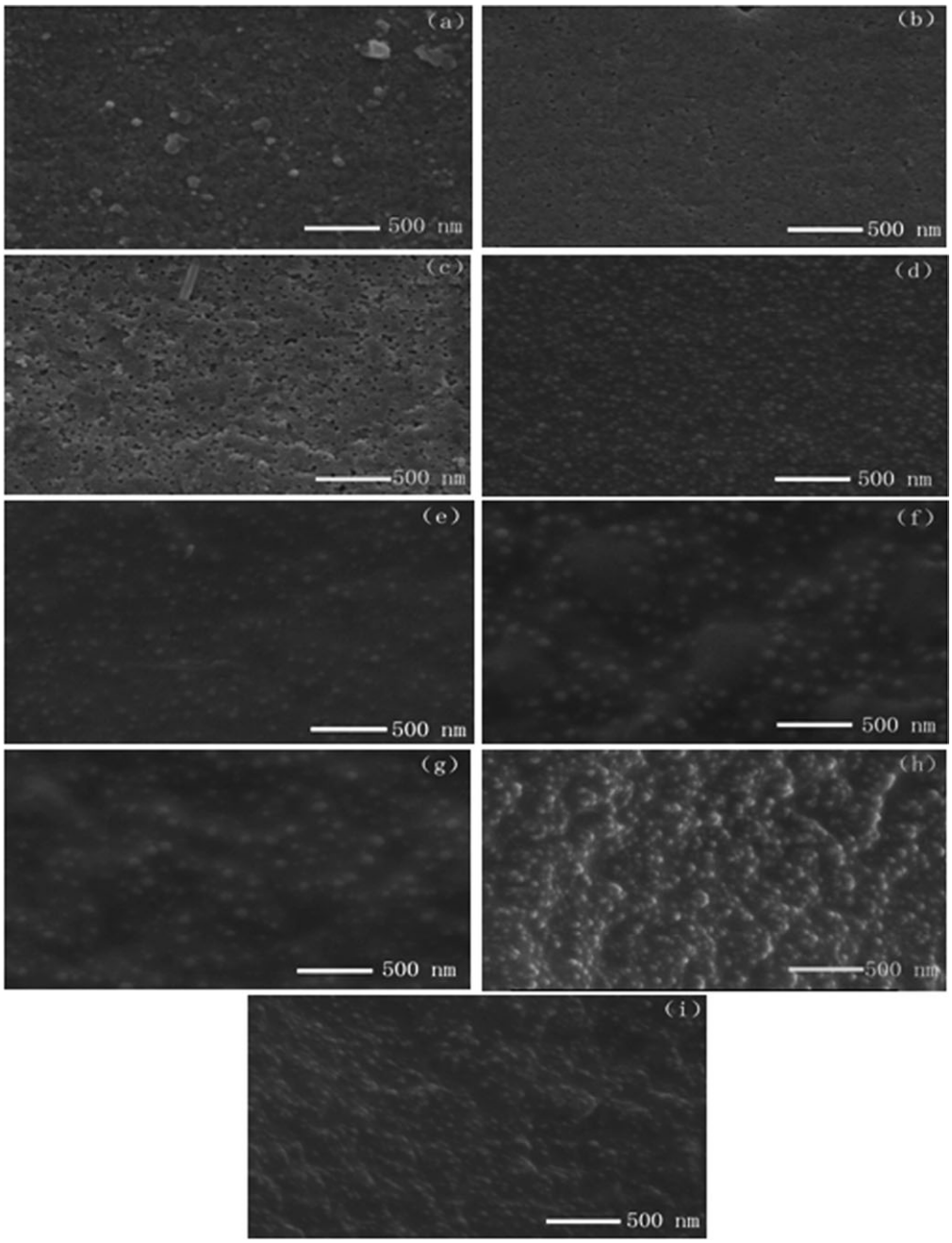

Figure 5. SEM images of upper surfaces of (a) S8/P6, (b) S14/P6, (c) S20/P6, (d) S30/P6, (e) S50/P6, (f) S80/P6, and (g) S100/P6 films and cross-section of (h) S14/P6 and (i) S30/P6 films at $f = 0.5$.

The film transparency of blends is related to three main factors: differences in the refractive indices among components, phase size, and the size and number of voids in films.[2,4] Generally, the difference in refractive index (RI) between silica (RI = 1.46) and polymer (RI = 1.47 − 1.49[3]) is small and does not seriously reduce the transparency of the blend films. For silica/polymer blend films with high silica loads, silica particles form gels easily, leading to macro phase separation. Because of the small difference in the refractive index of silica and that of polymer, macro phase separation also does not impact the transparency of blended films. In this way, film transparency mainly depends on voids, especially on the large voids caused by random packing of colloidal silica particles. When most of the voids are filled in by polymer chains, the resulting film is transparent. Otherwise, it becomes translucent or even turbid. At lower silica fractions, only low numbers of voids were produced. Those voids can be completely filled with polymer, so the process produces transparent films despite silica size. Higher silica fractions inevitably cause more voids. Nevertheless, the sizes of voids may be small enough not to scatter light for silica particles with small sizes (8, 14, and 20 nm). As a result, the blended film remains transparent, although the voids are not completely filled.

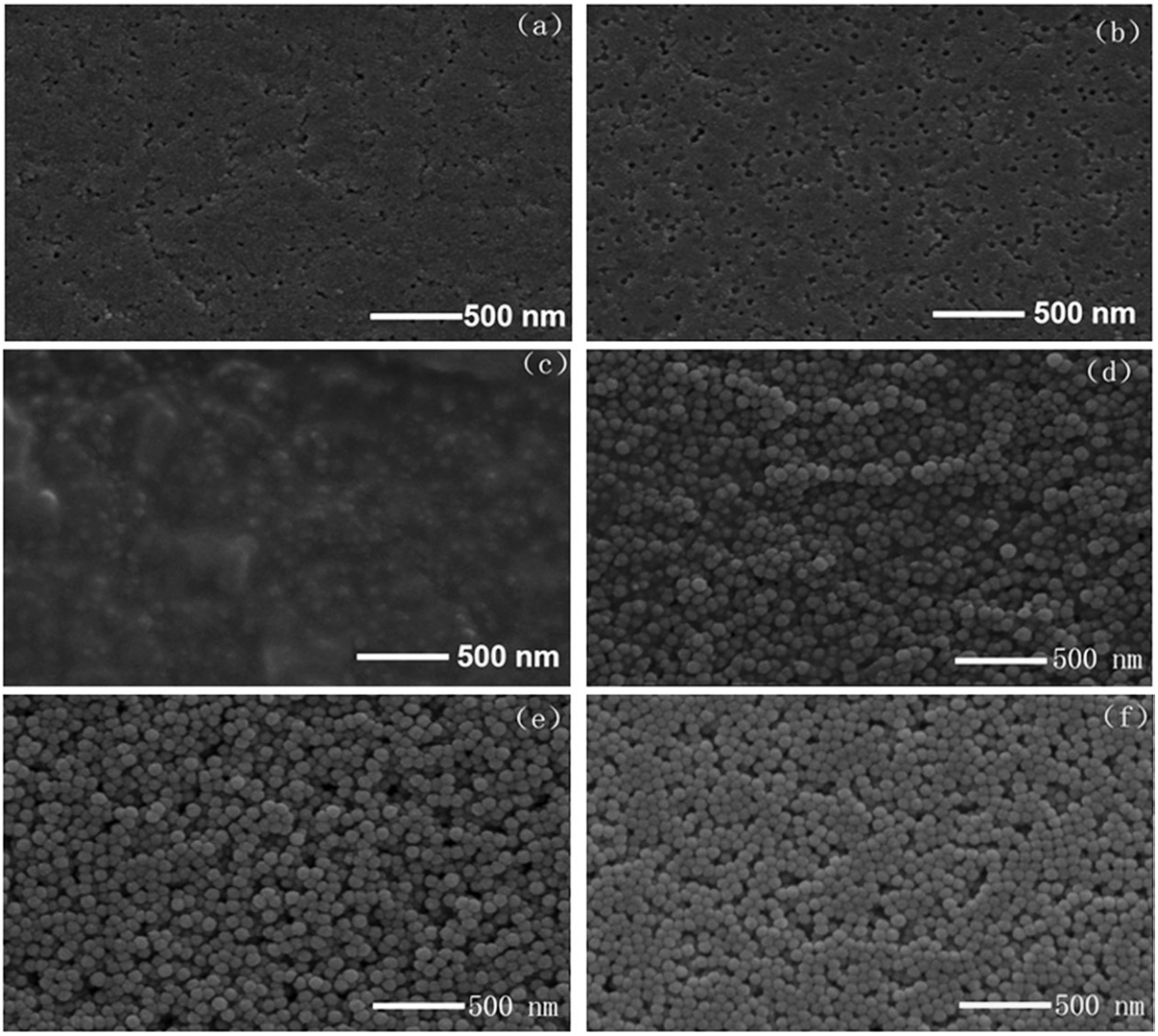

Figure 6. SEM images of top surface of silica/polymer nanocomposite films at various silica fractions: (a) S14/P6, $f = 0.6$, (b) S14/P6, $f = 0.7$, (c) S50/P6, $f = 0.6$, (d) S50/P6, $f = 0.7$, (e) S50/P6, $f = 0.8$, and (f) S50/P6, $f = 0.9$.

However, large voids are formed from random packing of big colloidal silica particles and thus translucent film.

Effect of T_g of Polymer Latex. Figure 4 demonstrates the film-forming ability of the latex blends prepared from S14 (or S50) silica sol and polymer latexes with various T_gs (P-22, P-3, P1, P12, and P25). The S14/polymer film started to crack but film transparency did not decrease as f increased, which was not affected by the T_g of the polymer. However, S50/polymer films turned opaque and then cracked as f increased. This is consistent with the film-forming phenomena that we observed in silica sol/P6 latex blends: small colloidal silica particles did not produce translucent films (as indicated by the overlapping f_1/f_2 curves), but large colloidal silica particles did (as indicated by the well-separated f_1/f_2 curves) at high silica loads.

Figure 4 shows that f_1 decreased slightly for both S14/polymer blends and S50/polymer blends as T_g increased. This means that softer polymer particles can release stress more efficiently. This is consistent with results observed for hard polymer/soft polymer latex blends.[2] In addition, f_2 remained nearly constant for S50/polymer latex blends as T_g changed. These results were similar to those observed for the blend of P6 latex and various silica sols. This could be explained by the fact that the volume of the voids was not impacted by the T_g of the polymer. It should be noted that the surfactants in the above latices with various T_gs were not removed in order to match their real applications. Since surfactant was demonstrated to play a major role on film-formation of polymer latex,[3,34] the above film-forming behavior may be impacted more or less by the existed surfactants.

Morphology

The SEM images of the upper surfaces of nanocomposite films made from P6 latex with various silica sols at $f = 0.5$ are presented in Figure 5. Some pores were observed at the surfaces of S8/P6, S14/P6, and especially S20/P6 nanocomposite films, which were the films with small silica particles (size <30 nm).

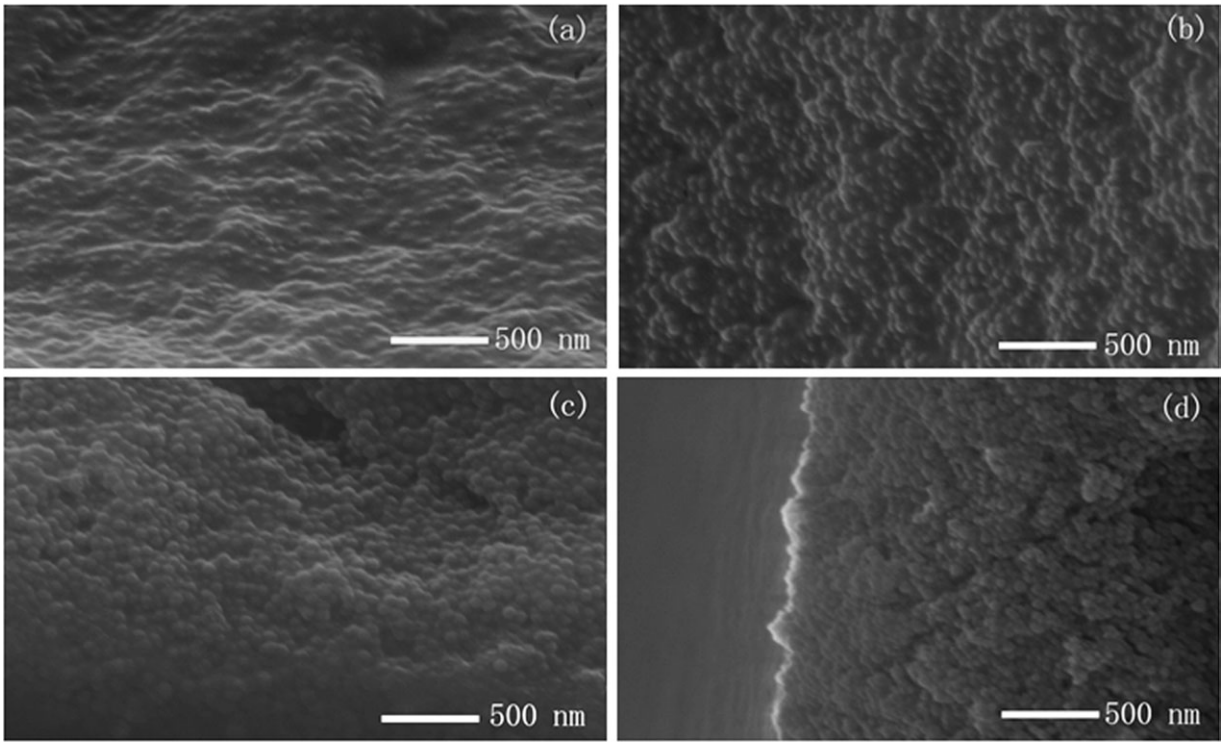

Figure 7. SEM images of cross-section of S50/P6 nanocomposite films at various silica fractions: (a) $f = 0.5$, (b) $f = 0.6$, (c) $f = 0.7$, and (d) $f = 0.8$.

These films were also flat in shape. No colloidal silica particles were found at their surfaces. However, particles rather than pores were found at the surfaces of the other nanocomposite films, which were prepared with large silica particles (size $\geq$30 nm). These particles were individually dispersed and could be considered as colloidal particles. The bulk morphology was typically examined for S14/P6 and S30/P6 films. Their cross-section SEM images are given in Figure 4. Both samples were dense nearly throughout. No pores were observed, but some were found at the surface of the S14/P6 film. This suggests that pores are distributed only on the upper surfaces of the films.

Porous surfaces have never before been observed in films made from blends of hard and soft polymer particles.[1,3,4,6] However, pores have been reported in composite films prepared from poly(St-*co*-BA-*co*-AA)/silica nanocomposite dispersion via forced-drying.[35] In this case, the silica content of the films was less than 20 wt %, and drying temperatures of up to 120°C were employed. The current study suggests that porous surfaces can be produced at high silica loads and room-temperature drying conditions. Its formation mechanism may be interpreted as follows. When the water in the silica/polymer wet film evaporates, polymer latex particles begin to randomly copack with colloidal silica particles. For those cases with silica size less than polymer latex size, the polymer latex particles are more possible to be completely blocked by the silica particles. Namely, some of polymer particles are individually dispersed in the silica particle matrix. If the polymer particle is distributed at the surface of the film, transfer of polymer chains from polymer latex particles to the voids of the silica framework takes place in order to minimize the surface energy of the film, finally leaving pores at the origin position of the polymer latex particles. The low T_g (6°C) of P6 latex can assure its mobility at room temperature. This formation mechanism of pores is similar to that of the polymer/silica films prepared via "forced drying" strategy.[18,35] However, the cases reported previously have much lower silica/polymer size ratio and higher drying temperature. All polymer latex particles can be blocked by silica particles and the silica particles network formed at high temperature are strong enough to reduce the film shrinkage during drying, and thus highly porous films are formed ultimately in those cases.[18,35]

Figure 6 shows the effect of f on the surface morphology of crack-free S14/P6 and S50/P6 nanocomposite films. As f increases, more pores occur at the surface of S14/P6 films. The greater number of voids in silica network allows more polymers to infiltrate the film, causing highly porous surfaces at higher values of f. As for S50/P6 films, the surface at $f = 0.6$ is rougher than that at $f = 0.5$ (Figure 5e). Nevertheless, this film still shows a continuous polymer phase. The polymer phase is difficult to see at $f = 0.7$ and invisible at $f = 0.8$ and 0.9. This morphological change alongside f is analogs to that of pigmented coatings. Herein, 0.7 of f just corresponds to the critical pigment volume concentration (CPVC). It is well known that polymer phase is not continuous and voids occur in the dried pigmented coatings above CPVC. The morphology of the cross-section of the films was further inspected for the S50/P6 films, as shown in Figure 7. It can be seen that the bulk morphologies of the films are very

Applied Polymer SCIENCE

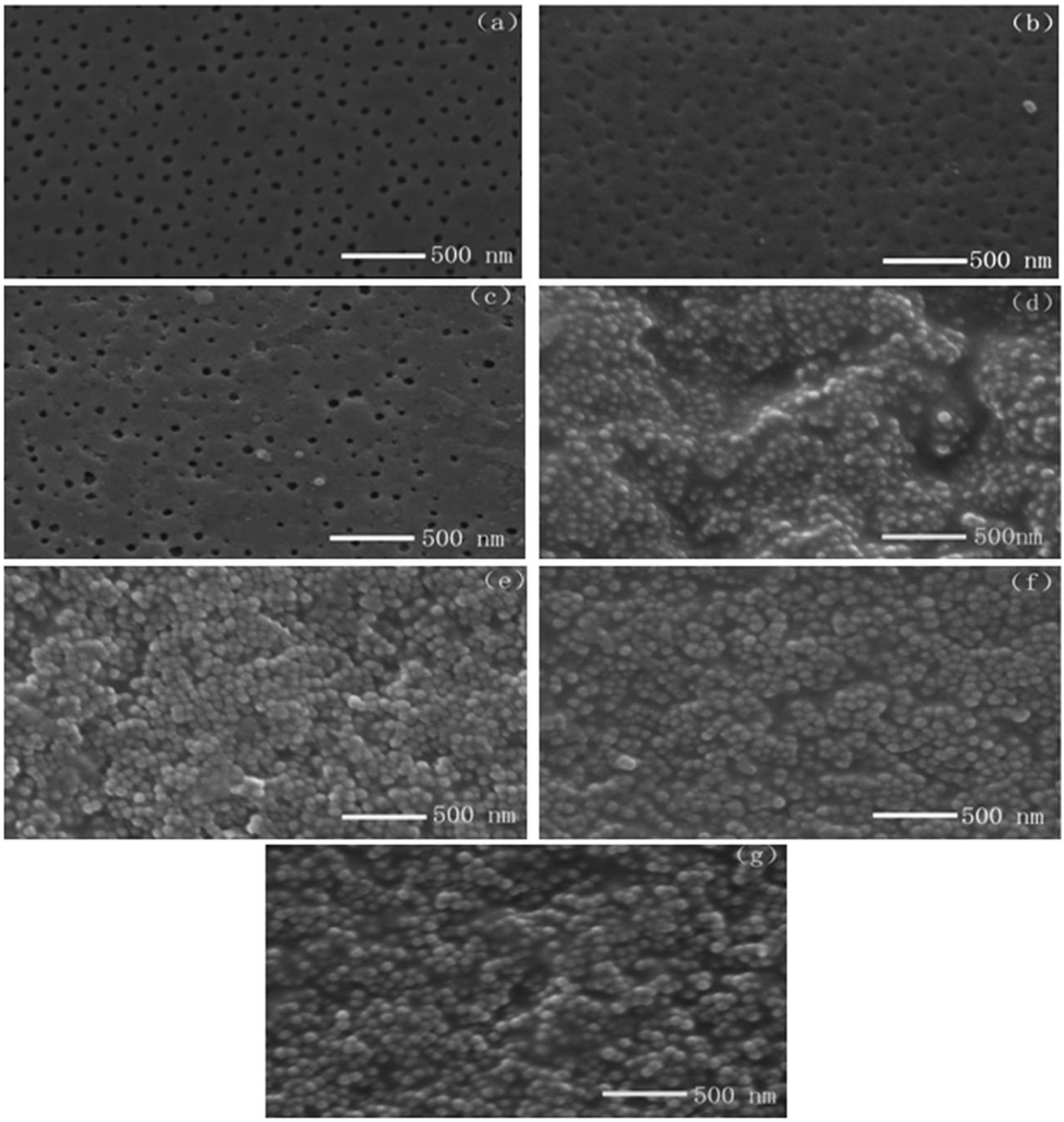

Figure 8. SEM images of the upper surfaces of silica/polymer nanocomposite films: (a) S14/P-3, $f = 0.5$, (b) S14/P-3, $f = 0.6$, (c) S14/P25, $f = 0.5$, (d) S50/P-22, $f = 0.5$, (e) S50/P1, $f = 0.5$, (f) S50/P12, $f = 0.5$, and (g) S50/P25, $f = 0.5$.

analogs to their corresponding surface morphologies. Voids also existed in the bulk of the film especially at $f = 0.8$. Therefore, the reduced transparency of the S50/P6 film at $f \geq 0.7$ should be due to voids that are not filled with sufficient amounts of polymer at high f.

The SEM images of the upper surfaces of nanocomposite films prepared with silica sol S14 (or S50) and large polymer latex particles (P-22–P25) are illustrated in Figure 8. Porous surfaces were revealed for S14/P-3 and S14/P25 films. Some immature pores were also observed for the S14/P-3 and S14/P25 films at $f = 0.5$, which may have been caused by the limited volume of voids in the silica framework. At $f = 0.5$, the S14/P-3 and S14/P25 films have larger pores than the S14/P6 film (Figure 5b). This confirms that the pores are caused by the transfer of polymer chains from polymer latex particles. The surface morphologies of S50/P-22, S50/P1, S50/P12, and S50/P25 films at $f = 0.5$ were similar. Colloidal silica particles were clearly visible, but polymers still made up the continuous phase, explaining the transparency of the films. The T_g of polymer latex was not found to affect the morphology of silica/polymer nanocomposite films.

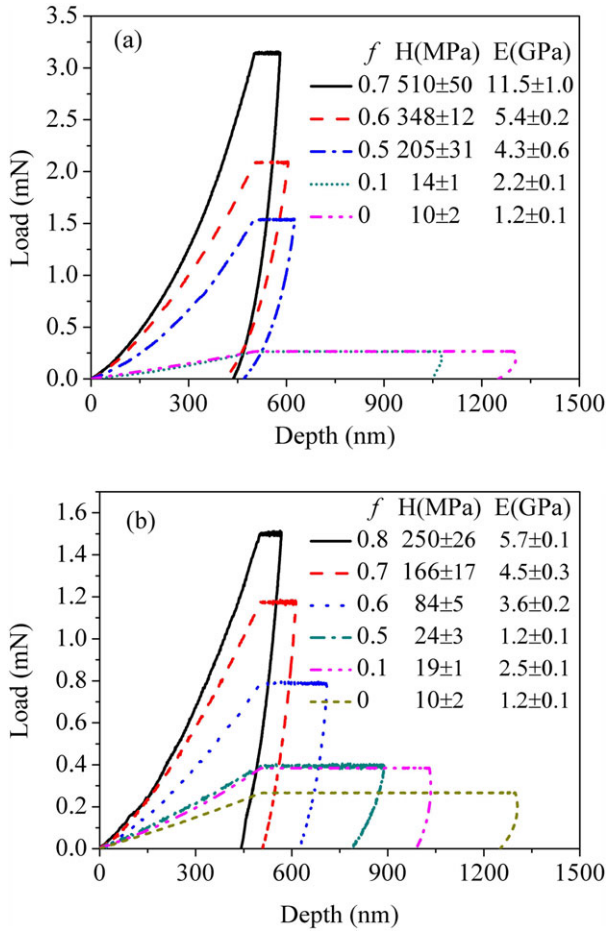

Figure 9. Loading-hold-unloading curves of (a) S14/P6 and (b) S30/P6 nanocomposite films prepared at different silica fractions. [Color figure can be viewed in the online issue, which is available at wileyonlinelibrary.com.]

Mechanical Properties, as Determined by Nanoindentation Tests

The loading-hold-unloading curves of S14/P6 and S30/P6 nanocomposite films with various silica fractions are shown in Figure 9. Pure P6 latex film exhibited severe creeping, extremely low reflow capability, and poor ability to resist deformation, indicating that the film was soft and viscous. The addition of small amounts of silica sol (10% S14 or S30) did not produce any obvious changes in its viscous-elastic behavior. However, in S14/P6 composite films the maximum load required to reach the designed penetration depth (500 nm) increased and creeping decreased as f increased to $f \geq 0.5$. Similar phenomena were also observed for S30/P6 composite films. However, the increasing degree of maximum load was much lower and creeping was more severe than in S14/P6 nanocomposite film at the same silica load. The S30/P6 nanocomposite films also displayed lower recovery after unloading than with S14/P6 nanocomposite films.

The microhardness and elastic modulus of these films are given in Figure 9. Substantial increments of microhardness and elastic modulus were revealed at $f \geq 0.5$ for S14/P6 films and at $f \geq 0.6$ for S30/P6 film. Values of 0.5 and 0.6 were found to be the critical silica loads for S14/P6 and S30/P6 films, respectively. As silica load increased, both microhardness and elastic modulus increased slightly while the silica load remained below the critical level; however, when the silica load was above the critical level, considerably increases were observed. As shown in Figure 9, S14/P6 films have much more pronounced microhardness and elastic modulus than S30/P6 films at the same silica load, and even than S30/P6 films with higher silica loads (e.g., S30/P6 films at $f = 0.6$ and 0.7 vs. S14/P6 film at $f = 0.5$). The most significant mechanical difference was caused by the differences in the strength of their silica frameworks. As mentioned above, during film formation smaller silica particles, here S14, can form strong silica networks. In contrast, colloidal silica particles, S30, tend to act as filler and form relatively weak silica aggregates.

Figure 10 shows the microhardness and elastic modulus of silica/polymer nanocomposite film as a function of silica size at $f = 0.5$ and 0.7. Microhardness decreased and then levels off as silica size increases for the films at both $f = 0.5$ and $f = 0.7$. Interestingly, the turning point at silica size of 30 nm just corresponds to the critical silica size for various film-forming behaviors. The greater hardness of nanocomposite films formed from smaller silica particles may be due to the formation of stronger silica skeletons in the film. When silica size exceeded the critical size, the colloidal silica particles mainly acted as filler, decreasing microhardness and weakening dependence on silica size. Abnormal trends were observed for films prepared with 8 nm colloidal silica at $f = 0.5$. This may have been due to the existence of silica aggregates in the sol. The elastic modulus of the nanocomposite film changes in a complicated manner as colloidal silica size increases. The decrements of elastic modulus in the silica size range of 8–30 nm may be due to strength differences in silica networks, which was similar to the change observed in microhardness. The reason for the trend in silica size within the range of 30–100 nm remains unclear and merits further investigation.

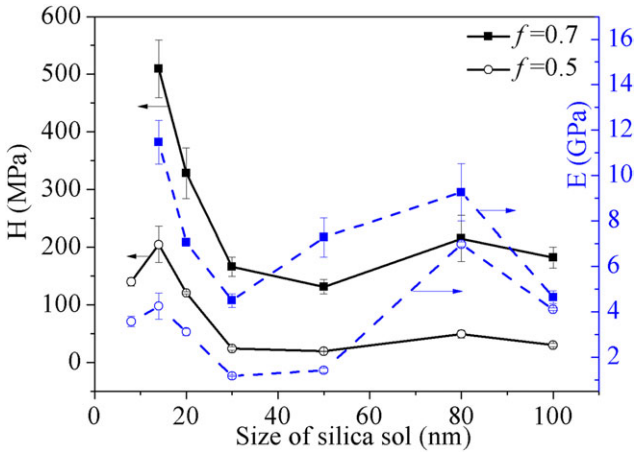

Figure 10. Microhardness and elastic modulus of silica/polymer nanocomposite films prepared from P6 latex and silica sols with various sizes. [Color figure can be viewed in the online issue, which is available at wileyonlinelibrary.com.]

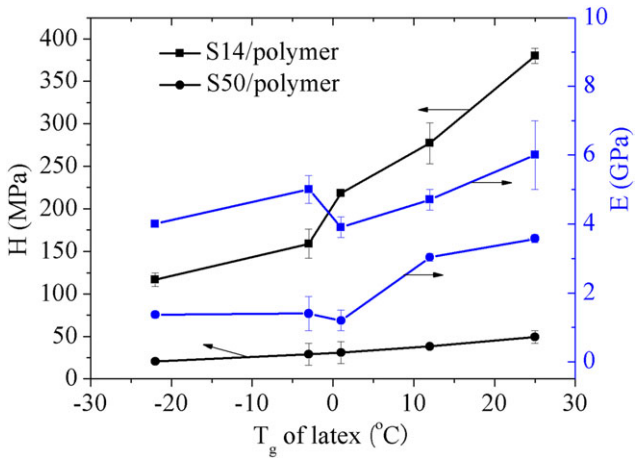

Figure 11. Influence of the T_g of the polymer on the microhardness and elastic modulus of S14- and S50-based nanocomposite films at $f = 0.5$. [Color figure can be viewed in the online issue, which is available at wileyonlinelibrary.com.]

The influence of the T_g of polymer latex on the mechanical properties of silica/polymer nanocomposite films is shown in Figure 11. In S14-based films, both microhardness and elastic modulus increased steadily as T_g increased. In S50-based films, hardness increased slightly as T_g increased, caused only by the polymer itself. Obvious enhancement of elastic modulus was found when the T_g of polymer exceeded 1°C. S14-based film was found to be superior to S50-based films with respect to mechanical properties regardless of T_g. This demonstrates that strong silica networks contribute greatly to the strength of the nanocomposite film.

CONCLUSION

Stable silica/polymer latex blends with silica mass fractions over 0.5 were fabricated using silica sols ranging in size from 8 to 100 nm and polymer latexes with T_g below room temperature. The maximum silica fraction of 0.7 for formation of crack-free transparent nanocomposite film was found to be achievable at room temperature using nanolatex with low T_g. Therefore, environment-friendly (i.e., waterborne) and cheap routes to get silica-riched nanocomposite coatings for potential applications in scratch resistant coatings, flame-retard coatings, low CTE coatings, and so on are feasible.

Thirty nanometers was found to be the critical silica size for the film-forming behavior, morphology, and mechanical properties. At silica sizes below 30 nm, the nanocomposite films cracked as silica load increased but did not show any deterioration in film transparency. They had porous surfaces and significant mechanical strength. When the silica size was greater than or equal to 30 nm, films transitioned from transparent to translucent film as silica load increased before finally cracking. The surface morphology of dried film was found to change with increases in silica load in a manner similar to pigmented coatings. The mechanical strength of the nanocomposite film was found to be inferior to that of films prepared with small silica particles. The formation of the silica framework was responsible for the morphological and mechanical differences among films with various silica sizes. Colloidal silica particles smaller than 30 nm were found to act as binders via the condensation of their surface silanol groups, forming strong silica skeletons. Colloidal silica particles larger than 30 nm tended to act as nanofiller rather than as binders. This film-forming behavior is somewhat different from that reported in hard/soft polymer latex blend. It should be universal for these latex blends that the hard particles can strongly interact with each other.

The critical silica load for the mechanical strength of silica/polymer film was exhibited. Above this critical silica load, nanocomposite films were hard with high elastic modulus. The higher the silica load, the more pronounced the hardness and elastic modulus of the film.

ACKNOWLEDGMENTS

This work is financially supported by Nature Science Foundation of China (Grant No. 51073038), the innovative team of Ministry of Education of China (Grant No. IRT0911) and Key Project of Nature Science Foundation of China (Grant No. 51133001).

REFERENCES

1. Eckersley, S. T.; Helmer, B. J. *J. Coat. Technol.* **1997**, *69*, 97.
2. Lepizzera, S.; Lhommeau, C.; Dilger, G.; Pith, T.; Lambla, M. *J. Polym. Sci. Part B Polym. Phys.* **1997**, *35*, 2093.
3. Feng, J.; Winnik, M. A.; Shivers, R. R.; Chubb, B. *Macromolecules* **1995**, *28*, 7671.
4. Tzitzinou, A.; Keddie, J. L.; Geurts, J. M.; Peters, A. C. I. A.; Satguru, R. *Macromolecules* **2000**, *33*, 2695.
5. Pauchard, L.; Abou, B.; Sekimoto, K. *Langmuir* **2009**, *25*, 6672.
6. Colombini, D.; Hassander, H.; Karlsson, O. J.; Maurer, F. H. J. *Macromolecules* **2004**, *37*, 6865.
7. Chevalier, Y.; Hidalgo, M.; Cavaillé, J.-Y.; Cabane, B. *Macromolecules* **1999**, *32*, 7887.
8. Luo, H.; Cardinal, C. M.; Scriven, L. E.; Francis, L. F. *Langmuir* **2008**, *24*, 5552.
9. Schmid, A.; Scherl, P.; Armes, S. P.; Leite, C. A. P.; Galembeck, F. *Macromolecules* **2009**, *42*, 3721.
10. Fielding, L. A.; Tonnar, J.; Armes, S. P. *Langmuir* **2011**, *27*, 11129.
11. Kobayashi, M.; Rharbi, Y.; Brauge, L.; Cao, L.; Winnik, M. A. *Macromolecules* **2002**, *35*, 7387.
12. Wada, T.; Inui, K.; Uragami, T. *J. Appl. Polym. Sci.* **2006**, *101*, 2051.
13. Wada, T.; Uragami, T. *J Coat Technol. Res.* **2006**, *3*, 267.
14. Liao, W. B.; Qu, J. Q.; Li, Z.; Chen, H. Q. *Chin. J. Chem. Eng.* **2010**, *18*, 156.
15. You, B.; Wen, N. G.; Cao, Y. C.; Zhou, S. X.; Wu, L. M. *Polym. Int.* **2009**, *58*, 519.
16. You, B.; Shi, L.; Wen, N. G.; Wu, L. M.; Zi, J. *Macromolecules* **2008**, *41*, 6624.
17. You, B.; Wen, N. G.; Shi, L.; Wu, L. M.; Zi, J. *J. Mater. Chem.* **2009**, *19*, 3594.

18. Zhang, S. L.; Zhou, S. X.; You, B.; Wu, L. M. *Macromolecules* **2009**, *42*, 3591.
19. Pagliaro, M.; Ciriminna, R.; Palmisano, G. *J. Mater. Chem.* **2009**, *19*, 3116.
20. Chan, C. M.; Cao, G. Z.; Fong, H.; Sarikaya, M.; Robinson, T.; Nelson, L. *J. Mater. Res.* **2000**, *15*, 148.
21. Messori, M.; Toselli, M.; Pilati, F.; Fabbri, E.; Fabbri, P.; Busoli, S.; Pasquali, L.; Nannarone, S. *Polymer* **2003**, *44*, 4463.
22. Kashiwagi, T.; Morgan, A. B.; Antonucci, J. M.; VanLandingham, M. R.; Harris, R. H.; Awad, W. H.; Shields, J. R. *J. Appl. Polym. Sci.* **2003**, *89*, 2072.
23. Mascia, L.; Kioul, A. *J. Mater. Sci. Lett.* **1994**, *13*, 641.
24. Sulaiman, S.; Brick, C. M.; Sana, C. M. D.; Katzenstein, J. M.; Laine, R. M.; Basheer, R. A. *Macromolecules* **2006**, *39*, 5167.
25. Uma, T. *J. Mater. Chem.* **2011**, *21*, 456.
26. Elodie, B. L.; Lansalot, M. *Adv. Polym. Sci.* **2010**, *233*, 53.
27. Martinez, C. J.; Lewis, J. A. *Langmuir* **2002**, *18*, 4689.
28. Singh, K. B.; Deoghare, G.; Tirumkudulu, M. S. *Langmuir* **2009**, *25*, 751.
29. Pharr, G. M.; Oliver, W. C.; Brotzen, F. R. *J. Mater. Res.***1992**, *7*, 1564.
30. Caddock, B. D.; Hull, D. *J. Mater. Sci.* **2002**, *37*, 825.
31. Nawaz, Q.; Rharbi, Y. *Macromolecules* **2008**, *41*, 5928.
32. Chiu, R. C.; Garino, T. J.; Cima, M. J. *J. Am. Ceram. Soc.* **1993**, *76*, 2257.
33. Dufresne, E. R.; Corwin, E. I.; Greenblatt, N. A.; Ashmore, J.; Wang, D. Y.; Dinsmore, A. D.; Cheng, J. X.; Xie, X. S.; Hutchinson, J. W.; Weitz, D. A. *Phys. Rev. Lett.* **2003**, *91*, 224501.
34. Wang, Y.; Kats, A.; Juhue, D.; Winnik, M. A.; Shivers, R.; Dinsdale, C. *Langmuir* **1992**, *8*, 1435.
35. You, B.; Wen, N. G.; Zhou, S. X.; Wu, L. M.; Zhao, D. Y. *J. Phys. Chem. B* **2008**, *112*, 7706.